Intratumoral injection of a CpG oligonucleotide reverts resistance to PD-1 blockade by expanding multifunctional CD8$^+$ T cells

Shu Wang[a,1], Jose Campos[a,1], Marilena Gallotta[a], Mei Gong[a], Chad Crain[a], Edwina Naik[a], Robert L. Coffman[a,2], and Cristiana Guiducci[a,2]

[a]Discovery, Dynavax Technologies Corporation, Berkeley, CA 94710

Contributed by Robert L. Coffman, September 30, 2016 (sent for review May 31, 2016; reviewed by Wolf Fridman and Miriam Merad)

Despite the impressive rates of clinical response to programmed death 1 (PD-1) blockade in multiple cancers, the majority of patients still fail to respond to this therapy. The CT26 tumor in mice showed similar heterogeneity, with most tumors unaffected by anti–PD-1. As in humans, response of CT26 to anti–PD-1 correlated with increased T- and B-cell infiltration and IFN expression. We show that intratumoral injection of a highly interferogenic TLR9 agonist, SD-101, in anti–PD-1 nonresponders led to a complete, durable rejection of essentially all injected tumors and a majority of uninjected, distant-site tumors. Therapeutic efficacy of the combination was also observed with the TSA mammary adenocarcinoma and MCA38 colon carcinoma tumor models that show little response to PD-1 blockade alone. Intratumoral SD-101 substantially increased leukocyte infiltration and IFN-regulated gene expression, and its activity was dependent on CD8$^+$ T cells and type I IFN signaling. Anti–PD-1 plus intratumoral SD-101 promoted infiltration of activated, proliferating CD8$^+$ T cells and led to a synergistic increase in total and tumor antigen-specific CD8$^+$ T cells expressing both IFN-γ and TNF-α. Additionally, PD-1 blockade could alter the CpG-mediated differentiation of tumor-specific CD8$^+$ T cells into CD127^{low}KLRG1^{high} short-lived effector cells, preferentially expanding the CD127^{high}KLRG1^{low} long-lived memory precursors. Tumor control and intratumoral T-cell proliferation in response to the combined treatment is independent of T-cell trafficking from secondary lymphoid organs. These findings suggest that a CpG oligonucleotide given intratumorally may increase the response of cancer patients to PD-1 blockade, increasing the quantity and the quality of tumor-specific CD8$^+$ T cells.

PD-1 blockade | TLR9 agonist | multifunctional CD8$^+$ T cells

In patients with solid tumors, biomarkers suggesting engagement of the immune system with tumor antigens within the tumor microenvironment have been shown to correlate with the patient response to blockade of programmed death 1 (PD-1) or programmed death ligand 1 (PDL-1) (1). For example, patients responding to MPDL3280A, an anti–PD-L1 antibody, have higher expression of PD-L1 and IFN-γ on tumor-infiltrating immune cells at baseline (2), and melanoma patients with CD8$^+$ T cells at the invasive margin of the tumors at baseline were more likely to respond to the anti–PD-1 antibody, pembrolizumab (3). These studies demonstrate that the efficacy of PD-1/PD-L1 targeting therapies is highest in patients who have mounted a specific antitumor T-cell immune response before starting therapy, despite the inability of that response to adequately control tumor growth. Among tumor types with a clinically significant response to PD-1/PDL-1, the majority of patients do not respond and show little evidence of immune recognition of tumor cells. Agents capable of stimulating infiltration and functional activation of both T cells and antigen-presenting cells in such tumors could synergize with PD-1 blockade to increase the frequency of responding patients and expand the range of tumors treatable with PD-1 inhibitors. Such stimulatory agents have the potential to enhance the extent or durability of responses even in patients showing positive clinical benefit from anti–PD-1 alone.

In this study, we tested the hypothesis that immunomodulation at the tumor site with a TLR9 agonist, in animals undergoing concurrent anti–PD-1 therapy, would convert the injected lesions into a vaccine site reverting resistance to PD-1 blockade. Synthetic oligonucleotides with immunostimulatory CpG motifs (CpG-ODN) are excellent candidates for combination with PD-1 blockade. Studies in mice have demonstrated that CpG-ODN can control tumor growth by coordinated activation of both innate and adaptive responses, especially if administered intratumorally (IT) (4). Human studies combining radiation therapy and intratumoral CpG-ODN have shown efficacy in patients with indolent B-cell lymphomas (5) and cutaneous T-cell lymphoma (6).

Mice transplanted with the CT26 colon carcinoma cell line respond variably to anti–PD-1 treatment, with many showing no response to the agent. Control of tumor growth correlates strongly with expression of an IFN-regulated gene signature and substantial T-cell infiltration. Initiation of intratumoral treatment with the CpG-ODN, SD-101, leads to rapid infiltration and expansion of polyfunctional CD8$^+$ T cells, resulting in durable control of tumor growth in virtually all animals and systemic immunity effective against uninjected distant-site tumors.

Significance

Recent data suggest that patients harboring immunologically incompetent tumors fail to respond to programmed death 1 (PD-1) blockade. We have developed a mouse tumor model that mimics resistance found in human tumors, and we show that intratumoral injections of a high IFN-inducing CpG oligonucleotide, SD-101, can rapidly lead to durable rejection of anti–PD-1 nonresponder tumors and generate systemic immunity to untreated distant-site tumors. The change in tumor microenvironment caused by SD-101 leads to rapid T-cell infiltration and generation of multifunctional CD8$^+$ T cells. These studies provide significant insights into the synergy between PD-1 blockade and local TLR9 activation and provide the experimental support for clinical studies of combination therapy with PD-1 blockade and intratumoral SD-101.

Author contributions: S.W., R.L.C., and C.G. designed research; J.C., M. Gallotta, M. Gong, C.C., and E.N. performed research; S.W., J.C., R.L.C., and C.G. analyzed data; and S.W., J.C., R.L.C., and C.G. wrote the paper.

Reviewers: W.F., Immune Microenvironment and Tumours Laboratory, Cordeliers Research Center, INSERM UMRS872; and M.M., Mt. Sinai School of Medicine.

Conflict of interest statement: The authors are present or former employees of Dynavax Technologies, which supported this work and is conducting clinical trials of SD-101 for the treatment of lymphoma and melanoma.

Freely available online through the PNAS open access option.

[1]S.W. and J.C. contributed equally to this work.

[2]To whom correspondence may be addressed. Email: cguiducci@dynavax.com or RCoffman@dynavax.com.

This article contains supporting information online at www.pnas.org/lookup/suppl/doi:10.1073/pnas.1608555113/-/DCSupplemental.

Results

The Response of CT26 Tumors to PD-1 Blockade Correlates with T- and B-Cell Infiltration and Type I IFN. Groups of mice transplanted with CT26 colon carcinoma cells consistently show variation in the response to PD-1 blockade. Twenty-six out of 60 tumors responded completely (17%) or partially (>80% reduction in tumor volume, 26%) to five doses of anti–PD-1 (Fig. 1*A*). However, the majority of tumors (56%) were insensitive to anti–PD-1 treatment, growing at the rate of tumors in untreated mice. Tumors in anti–PD-1 responders contained an increased density of infiltrating leukocytes compared with unresponsive or untreated tumors (Fig. 1*B*). Reduction in tumor size in response to anti–PD-1 correlated strongly with elevated expression of genes regulated by type I IFNs and genes indicating T-cell presence and activation (Fig. 1*C*). A similar correlation was observed between tumor size and both immunoglobulins (IgH-6) and B-cell signature genes, including the B-cell chemoattractant chemokine, CXCL13 (7) (Fig. 1*C*). A similar level of heterogeneity in these signatures was observed in small tumors (day 7; 2–4 mm in diameter) before the start of anti–PD-1 treatment (Fig. 1*D*). Tumors showing the highest levels of T-cell-related genes also expressed high levels of gene signatures for types I and II IFNs and B-cell activation (Fig. S1*A*). These results suggest that the variation in immune contexture may be preexisting in this tumor model but do not exclude that it can be induced by anti–PD-1 treatment. Consistent with the central role of type I IFN in shaping the antitumor response (8), the response to PD-1 blockade was abrogated by a blocking antibody to the type I IFN receptor (Fig. 1*E*). To address whether B cells have a role in anti–PD-1 antitumor activity, mice treated with anti–PD-1 therapy were given a CXCL13 blocking antibody, which has been shown to decrease B-cell infiltration in tumors (9, 10) (Fig. S1*B*). The response to anti–PD-1 was significantly decreased in the presence of CXCL-13 blockade (Fig. 1*E*), suggesting that B cells contribute to anti–PD-1 activity, rather than simply being recruited by activated T cells and dendritic cells (DCs).

Intratumoral Immunomodulation with a High Interferogenic CpG Overcomes Resistance to PD-1 Blockade. The well-described activities of CpG-ODN suggest it may correct the deficiencies in IFN production and cellular composition observed in anti–PD-1 unresponsive tumors and increase the frequency of mice able to generate durable antitumor immunity. SD-101 is a palindromic CpG-C class ODN currently being evaluated for immunotherapy in lymphoma and melanoma, in combination with local irradiation or pembrolizumab, respectively. SD-101 administered by IT injection as a single agent in mouse tumors is pharmacologically active, as demonstrated by substantial inhibition of tumor growth (Fig. S2*A*) and elevation of type I IFN regulated genes in the tumor microenvironment (Fig. S2*B*); however, it did not lead to durable rejection in most treated animals (Fig. S2*A*). To evaluate whether treatment with SD-101 could convert anti–PD-1 nonresponders to responders, mice were randomized 12 d after initiation of anti–PD-1 therapy into two groups and injected IT with either SD-101 or an inactive non-CpG oligonucleotide (CTRL-ODN) while continuing anti–PD-1 treatment. SD-101 addition to anti–PD-1 led to tumor rejection in 100% of treated mice, whereas treatment with CTRL-ODN did not increase response rates compared with the rate with anti–PD-1 alone (Fig. 2 *A* and *B*). Both SD-101 and anti–PD-1 were required for this uniform tumor rejection, as mice with tumors similar in size but treated only with SD-101 showed transient inhibition of tumor growth, but tumors were not completely rejected, and all ultimately progressed (Fig. 2 *A* and *B*). Thus, the complete responses seen with combination therapy represent a synergistic interaction between anti–PD-1 and SD-101. Parallel studies using an anti–PD-L1 blocking antibody demonstrated comparable results (Fig. 2 *C* and *D*). In mice given CT26 tumors on both flanks and treated with anti–PD-1, SD-101 injection into one tumor site generated systemic immunity leading to rejection of both treated and untreated tumors and long-term survival in 13 out of 19 (68%) mice (Fig. 2*E*). Mice that rejected the tumors in response to SD-101 plus either anti–PD-1 or anti–PD-L1 rejected a rechallenge with CT26 cells 100 d after initial tumor inoculation, demonstrating the induction of immunological memory (not shown).

$CD8^+$ but not $CD4^+$ T cells were required, as a loss of therapeutic efficacy was observed only in mice depleted of $CD8^+$ T cells starting the day before the first SD-101 treatment (Fig. 2*F*). SD-101 stimulated the levels of IFNs and IFN-regulated genes in mice nonresponsive to anti–PD-1, bringing expression to levels comparable to anti–PD-1 responsive tumors (Fig. 2*G*). Blocking IFN signaling decreased the response to anti–PD-1 plus SD-101 treatment (Fig. 2*H*).

Similar studies were performed with two additional transplantable tumor models, the TSA mammary adenocarcinoma and the MCA38 colon carcinoma. Both models are more resistant to PD-1 blockade than CT26, as shown by a limited ability of anti–PD-1 to induce tumor rejection. SD-101 given to one site in anti–PD-1 treated mice bearing tumors on both flanks led to significant rates of tumor rejection in both the injected and uninjected tumor sites (Fig. 3 *A*–*D*), demonstrating the induction of systemic antitumor immunity in many animals. Thus, intratumoral administration of SD-101 can unmask the potential of PD-1/PD-L1 blockade by increasing IFN production and promoting a $CD8^+$ T-cell response able to clear treated and distant untreated tumors.

Synergistic Up-Regulation of Immune-Related Gene Signature by SD-101 in Combination with Anti–PD-1. To identify functional pathways associated with the response to anti–PD-1, SD-101, and the combination, microarray analysis was performed on three to four replicate pools of two to three CT26 tumors in each group (Fig. 4 *A* and *B*). Anti–PD-1-treated tumors were classified as responders (having at least 60% reduction in tumor volume) or nonresponders and analyzed separately. Tumors were collected after only three SD-101 injections to permit sufficient tissue to be collected from tumors undergoing rejection. The gene expression profiles of tumors from anti–PD-1 nonresponders and CTRL-ODN-treated tumors were indistinguishable; thus, subsequent comparisons were made primarily to the control subset. We focused subsequent analysis on respective contributions of SD-101 and anti–PD-1 to the synergistic antitumor response obtained with the combination, illustrated by the Venn diagram representing the overlap of differentially expressed genes (DEG) in tumors from all treatment groups versus tumors from controls (Fig. 4*C*). In the anti–PD-1 plus SD-101 group, there is an overall increase in the number of DEG (1,745) compared with the anti–PD-1 responder (821) or SD-101 monotherapy (950) groups. Nearly 30% of the DEG in each treatment group is predicted to be regulated by type I and/or type II IFNs (Fig. 4*D*), as classified in the Interferome database (11).

Advanced gene ontology (GO) analysis was carried out to identify biological processes represented by these changes in gene expression relative to the control group (Fig. 4*E*). The Venn diagram shows the number and overlap of significant GO terms. For each of the major patterns of overlap, the 12 most significant GO terms are listed, along with a graphical representation of the significance (by color) and the fraction of genes in each GO gene set differentially expressed (by length). A complete list of the GO terms is given in Fig. S3. The 35 GO terms significant only in anti–PD-1 responders are associated with humoral response, macrophage activation, and antigen processing and presentation. In contrast, the 27 GO terms common to all three treatment groups represent immune responses, leukocyte migration, chemokine production, and B-cell receptor signaling. The 12 GO terms common to anti–PD-1 responder and anti–PD-1 plus SD-101 groups are related to inflammatory response, cell adhesion, and

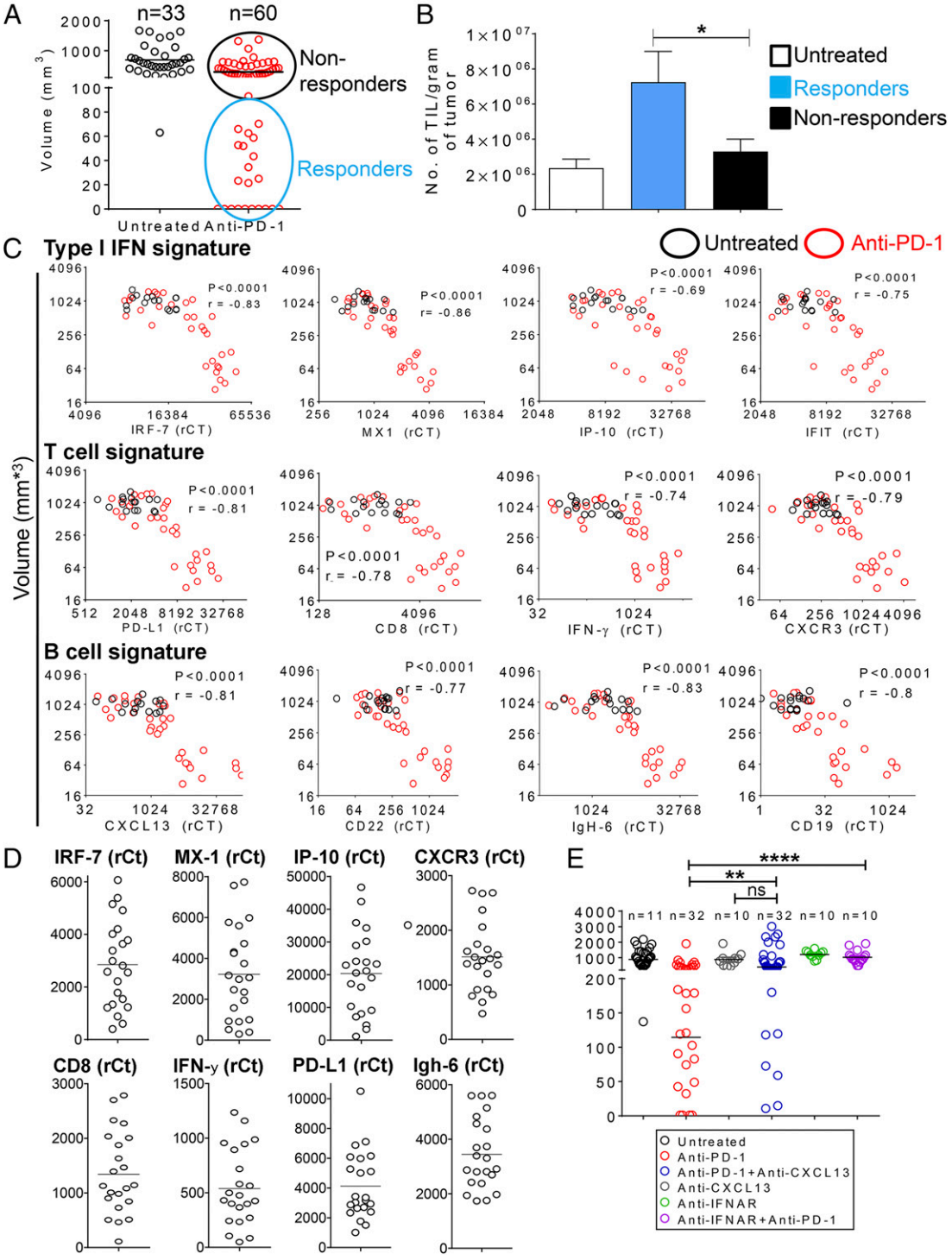

Fig. 1. Mice bearing CT26 tumor nodules produce a heterogeneous response to systemic PD-1 blockade. (*A*) Distribution of tumor nodule sizes after five anti–PD-1 injections. CT26 cells were injected s.c. at day 0 on both flanks. Anti–PD-1 was administered i.p. on days 5, 8, 11, 14, and 18. Tumor volumes were measured 4 d after the last injection. Data are pooled from two independent experiments. (*B*) Density of TILs in subset of tumors from *A*. Shown is the mean ± SEM based on: four untreated mice, seven anti–PD-1 nonresponders, and nine anti–PD-1 responders. $*P \leq 0.05$. (*C*) Response to anti–PD-1 correlates with type I IFN and T- and B-cell gene signatures. Tumors were harvested 4 d after the last anti–PD-1 injection, and gene expression was measured by TAQMAN gene expression. Cumulative data are from five independent experiments, with a total number of 16 in the untreated group and 32 in the anti–PD-1 group. Spearman's ρ was used to calculate the correlation between gene expression levels and tumor volumes. All statistical tests were two-sided, and *P* values ≤0.05 were considered significant. (*D*) Heterogeneity of IFN-regulated genes and T-cell and B-cell signature gene expression in early-established s.c. tumors. CT26 cells were injected s.c. at day 0 on both flanks, and tumors were harvested 7 d later for TAQMAN analysis. Data are pooled from two independent experiments ($n = 22$). (*E*) Volume distribution of tumors following anti–PD-1 blockade in the absence or presence of the interferon-α/β receptor (IFNAR) blocking Ab or CXCL13 blocking Ab. CT26 cells were injected s.c. at day 0 on both flanks. Anti–PD-1 blocking antibody was administered on days 8, 11, 13, 18, and 20. Tumor volume was measured 4 d after the last injection, at day 24. Data are pooled from two independent experiments. $**P \leq 0.01$; $****P \leq 0.0001$.

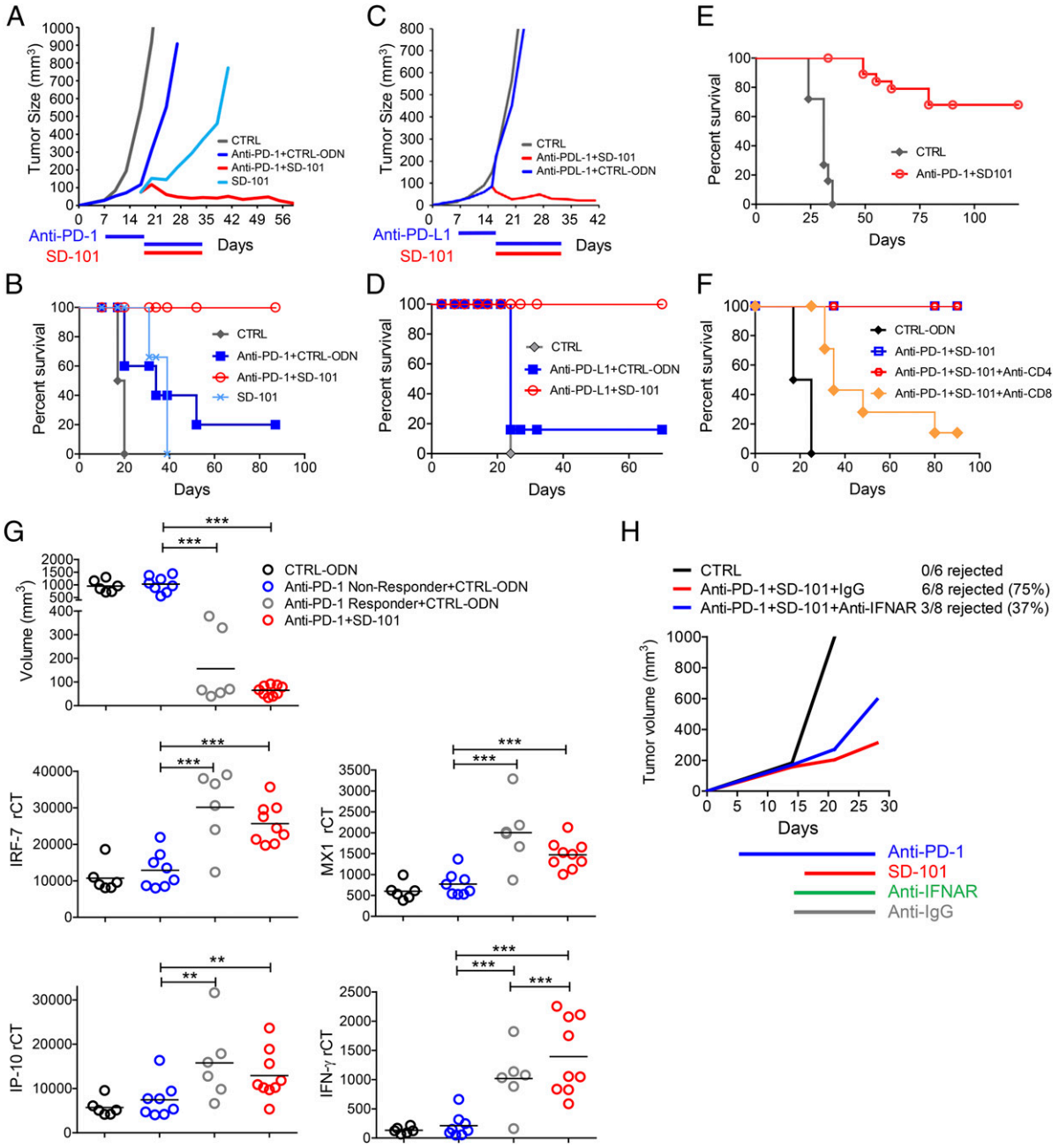

Fig. 2. Intratumoral SD-101 reverses tumor escape from anti–PD-1 therapy and leads to $CD8^+$ T-cell and IFNAR-mediated tumor rejection. (*A*) Graphical representation of mean tumor volumes over time. CT26 tumor cells were injected s.c. in the flank of mice on day 0. Anti–PD-1 treatment started when tumor reached 5 mm (day 7). Mice were left untreated, or mice were treated with i.p. injections of anti–PD-1 administered on days 7, 10, 14, 17, 21, 25, 28, and 32. After four anti–PD-1 injections (day 19), mice started receiving intratumoral injections of 50 μg of SD-101 or CTRL-ODN administered on days 19, 21, 25, 28, 32, and 35. A separate group of mice with similar tumor size but no pretreatment with anti–PD-1 received SD-101 alone. (*B*) Long-term survival of mice in *A*. One representative experiment of four experiments, each performed with four to eight mice per group, is shown. (*C* and *D*) SD-101 increases response to anti–PD-L1 treatment. (*C*) Tumor volumes over time. (*D*) Overall survival. Experiment was performed with a similar schedule to that used in *A* but using an anti–PD-L1 blocking Ab with six mice per group. (*E*) Anti–PD-1 plus SD-101 combination therapy allows for rejection of contralateral tumors. Survival of mice bearing two s.c. tumors (right and left flank) that received systemic anti–PD-1 and IT SD-101 only in the left tumors. CT26 cells were injected s.c. on day 0 in the left flanks and on day 3 in the right flanks. Experiments were performed with a similar schedule to that used for the anti–PD-1 blocking antibody in *A*. Cumulative data from two independent experiments are shown. CTRL group, $n = 18$; SD-101 plus PD-1 group, $n = 19$. (*F*) $CD8^+$ T cells but not $CD4^+$ T cells are required for the efficacy of anti–PD-1 plus SD-101 combination treatment. Graph represents survival of mice upon depletion of $CD8^+$ or $CD4^+$ T cells. Experiment was performed with a similar schedule to that used in *A*. Depletion antibodies were started the day before the start of SD-101 treatment and given every 3 d until the end of SD-101 treatment; $n = 7$ per group. (*G*) SD-101 treatment restores IFN production in anti–PD-1-treated tumors. Anti–PD-1 treatment was administered on days 5, 9, 12, 14, 19, and 22. After four anti–PD-1 injections (day 14), SD-101 or CTRL-ODN was started and administered on days 16, 19, and 22. TAQMAN analysis was performed on whole tumors harvested 4 d after the last treatment. (*G*, *Upper*) Graph shows the tumor size at time of excision. (*Lower*) Graphs show TAQMAN analysis. Cumulative data from two independent experiments are shown. $^{**}P \leq 0.01$; $^{***}P \leq 0.001$. (*H*) Blockade of IFNAR impairs tumor rejection in response to anti–PD-1 plus SD-101 combination treatment. Experiments were performed with a similar schedule to that used in *A*. IFNAR blocking Ab or anti-IgG control were started 1 d before the first SD-101 treatment and given every 3 d for the duration of SD-101 treatment.

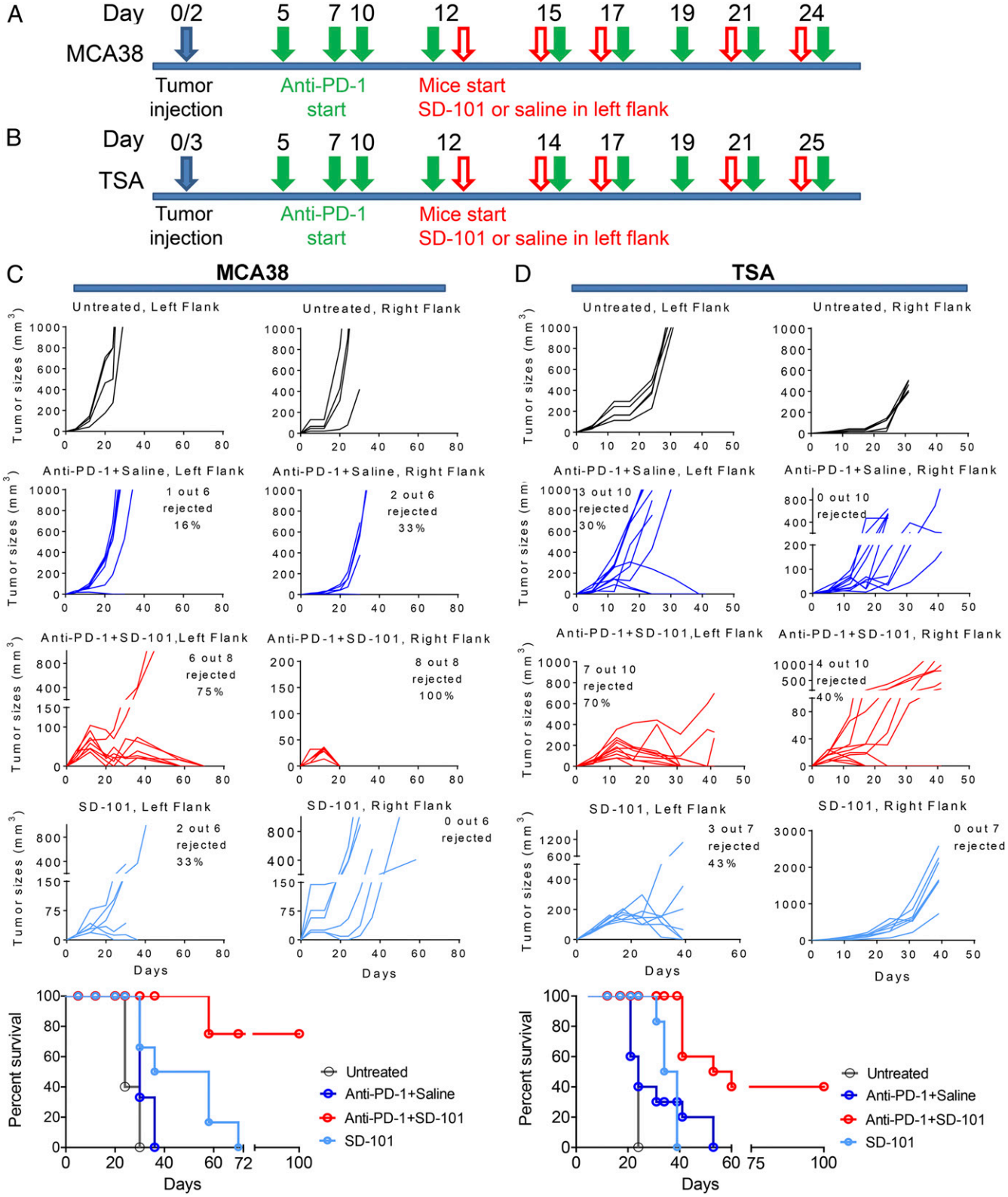

Fig. 3. SD-101 in combination with anti–PD-1 significantly improves the survival of mice bearing MCA38 colon carcinoma (*A*) and TSA mammary adenocarcinoma (*B*). Treatment schedule scheme is as follows: C57BL/6 or BALB/C mice were implanted s.c. on the left flank with either 7.5×10^4 MCA38 cells (*C*) or 3×10^5 TSA cells (*D*) on day 0, and on day 2 or 3 on the right flank. After four anti–PD-1 injections, mice were randomized and received SD-101 or CTRL-ODN only in the left flank; a separate group of mice with the same tumor size, not pretreated with anti–PD-1, started receiving intratumoral injection of SD-101 alone in the left flank. Mice were then followed for tumor growth and survival.

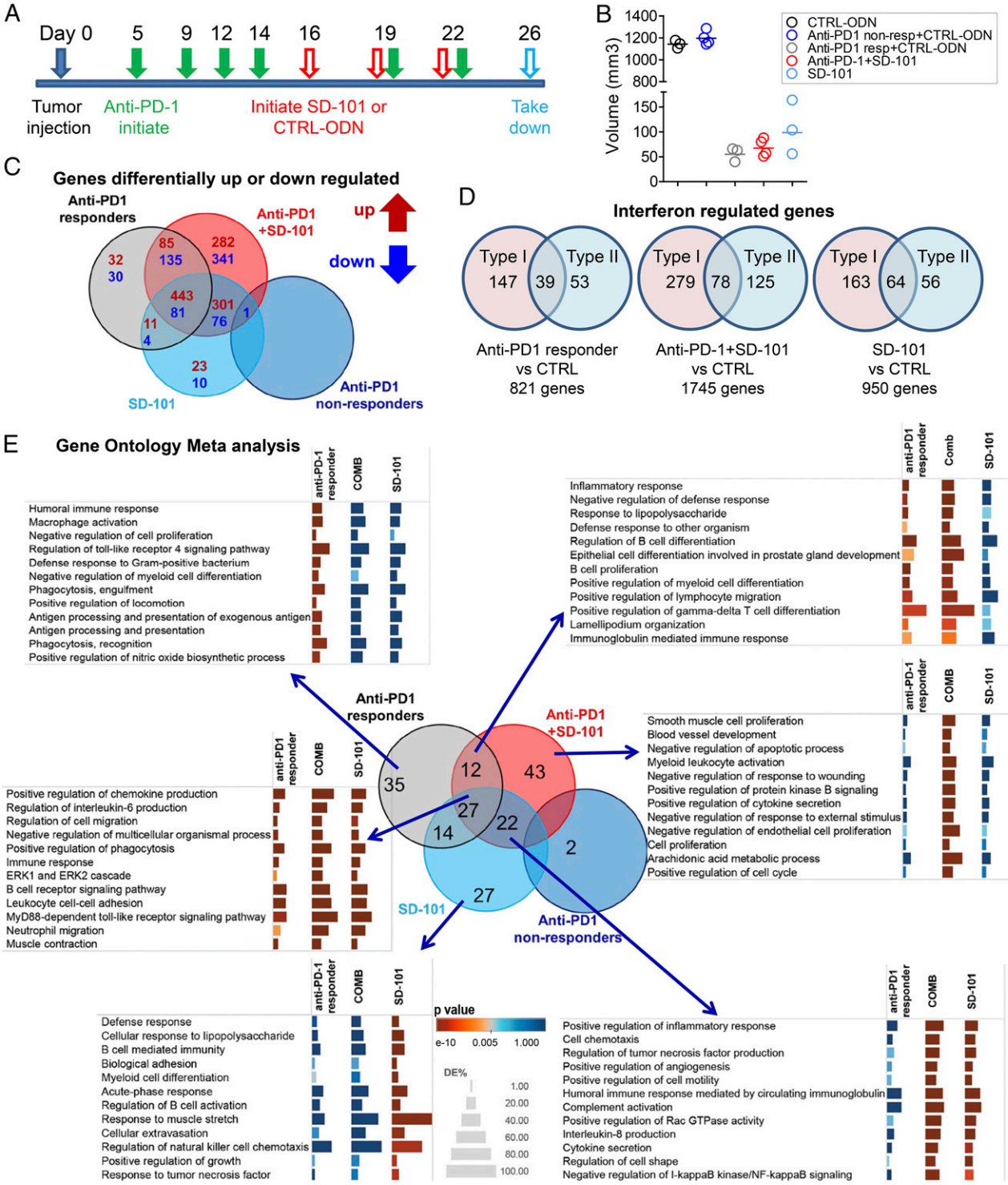

Fig. 4. Microarray analysis of tumors treated by anti–PD-1, SD-101, or the combination of anti–PD-1 and SD-101. (*A*) Treatment schedule scheme for microarray tumor samples: Anti–PD-1 treatment started 5 d after tumor cell inoculation. After four anti–PD-1 injections, mice were randomized and received three intratumoral injections of SD-101 or CTRL-ODN, with or without another two anti–PD-1 injections. A separate group of mice with the same tumor size but no pretreatment of anti–PD-1 started receiving SD-101 alone. SD-101 and CTRL-ODN were given every 3 d. Tumors were harvested 4 d after the last SD-101 or CTRL-ODN injection. (*B*). Mean volumes of tumor samples tested by gene expression microarray. Each sample is a pool of two to three tumors. Cumulative data from two independent experiments are shown. (*C*). Addition of SD-101 to anti–PD-1 expanded the Venn diagram of DEG (defined as ≥twofold difference in expression and a *P* value of <0.05) in tumors from all treatment groups versus tumors from CTRL-ODN–treated mice. Diagram was constructed using iPathway software. (*D*) Type I and type II IFN regulated genes in each contrast identified by Interferome database. Each contrast is the relative gene levels to the CTRL-ODN–treated group. (*E*) Venn diagram showing the overlap of the GO terms retrieved from term enrichment analysis performed using iPathway software; cut-off *P* value for selection of GO terms, $P < 0.005$. The fraction of DEG significance for selected immune-related GO terms was visualized by Tableau software. Enrichment significance is conveyed as bar color intensity. Height of the bar is proportional to the number of DEG in the GO terms. The *P* value is computed by iPathway software using hypergeometric distribution and is corrected using weight pruning.

B-cell proliferation and activation. Interestingly, among the GO genesets (27 + 12) common to anti–PD-1 responders with or without SD-101, the fraction of DEG was generally greater in tumors treated with both agents, consistent with the synergy observed in the antitumor activity. The gene signatures associated with humoral response are consistent with a significant increase of $GL7^+CD95^+$ germinal center B-cell infiltrating tumors treated with anti–PD-1 plus SD-101. These B cells expressed IgD, which may correspond to newly differentiated GC B cells (12) (Fig. S4), suggesting that the combined treatment promotes formation of intratumoral lymphoid structures.

SD-101 Combined with Anti–PD-1 Induces Accumulation of Polyfunctional T Cells with Increased Clonality. To characterize the effects of SD-101, anti–PD-1, and the combination on the tumor-infiltrating T cells (TILs), we isolated TILs from tumors undergoing anti–PD-1 treatment after three injections of SD-101 or CTRL-ODN (Fig. 5*A*). Tumors were harvested 4 d after last treatment at a time at which mice responding to treatments still had tumors of similar size, allowing a clear comparison of relative numbers and functional state of T cells among treatment groups (Fig. 5*B*). Treatment with either anti–PD-1 or SD-101 led to a substantial increase in the density (cells per gram of tumor) of $CD3^+CD8^+$ T cells, and also increased the proportion of $CD8^+$ T cells within the TILs (Fig. 5*C*). Combination treatment led to a significant increase in the density (cells per gram of tumor) of $CD3^+CD8^+$ T cells and also increased the proportion of $CD8^+$ T cells within the TILs (Fig. 5*C*) compared with all other groups. In contrast, we observed a decreased fraction of $CD3^+CD4^+$ T cells among $CD45^+$ cells in all three responding treatment groups relative to unresponsive tumors (Fig. 5*D*). This decrease was not due to a decreased percentage of Treg ($CD4^+FOXP3^+$) among $CD4^+$ T cells, which were equivalent in all treatment groups (Fig. 5*E*).

Proliferation and cytokine production after TCR (T-cell receptor) stimulation are among the first effector functions lost in TILs progressing through the stages of T-cell exhaustion (13, 14). In both single-treatment groups, the frequencies of proliferating K_i-67^+ $CD4^+$ and $CD8^+$ T cells were significantly increased, with an additive or synergistic increase observed in mice treated with both agents (Fig. 5*F*). Similarly, the fraction of $CD8^+$ T cells and $CD4^+$ T cells coexpressing both IFN-γ and TNF-α was greatly increased in the anti–PD-1 plus SD-101 treatment group compared with single-treatment or control groups (Fig. 5*G*). $CD8^+$ T cells specific for the endogenous CT26 antigen, gp70, detected by the AH1 dextramer, were significantly increased in the combined treatment group (Fig. 5*H*), and this $AH1^+$ population was also substantially enriched for double IFN-γ and TNF-α producing cells, relative to single-treatment groups (Fig. 5*I*). These results indicate that combined treatment promotes an increase in recruitment of $CD8^+$ T cells, many specific for tumor antigens, which proliferate and exhibit polyfunctionality, demonstrating a reversal of the exhausted phenotype of the TIL.

After antigen encounter, CD8 T cells can differentiate in short-lived effector cells (SLEC), which are terminally differentiated effector cells, and memory precursor effector cells (MPEC) which are long-lived effector cells destined to become memory cells (15). Tumors responding to anti–PD-1 alone or to the combination treatment harbor a significantly increased number of antigen-specific $CD8^+$ T cells with the MPEC phenotype, whereas the SD-101 alone-treated group is highly enriched in $CD8^+$ T cells with a SLEC phenotype (Fig. 5 *J* and *K*). To determine changes in the repertoire of infiltrating T cells, TCR-β sequences were assessed in tumors from mice treated with anti–PD-1 plus SD-101, or SD-101 alone, and compared with tumors from anti–PD-1 nonresponder mice. Tumors treated with SD-101 alone and the combination of anti–PD-1 plus SD-101 had a significantly increased clonality index, compared with the anti–PD-1 nonresponder group (Fig. 5*L*, *Right*), suggesting that SD-101 induced the expansion of a subset of T cells infiltrating the tumor, possibly by promoting cross-priming of tumor antigens. In addition, tumors treated with the combination had significantly higher richness, as measured by the number of T-cell clones with unique productive TCRs, compared with other groups (Fig. 5*L*, *Left*). The increase in richness of the repertoire is consistent with the increased $CD8^+$ T-cell accumulation in the combination treatment group (Fig. 5*C*) and suggests that the SD-101 plus anti–PD-1 combination promotes the expansion of previously rare, low-frequency T-cell clones. To understand whether the antitumor activity of the combined treatment was the result of new T-cell migration from draining lymph nodes or activation of T cells within the tumor, mice were treated with the sphingosine 1-phosphate receptor-1 antagonist, FTY720 (16, 17). FTY720 given 2 h before SD-101 depleted circulating T cells (Fig. S5*A*) but did not affect antitumor activity of the combined treatment (Fig. 5*M*). A similar increase in proliferating $CD8^+$ T cells in the tumor was observed with or without FTY720 (Fig. S5*B*), suggesting that priming and expansion of $CD8^+$ T cells can occur within the tumor itself. However, SD-101 does increase lymphocyte cellularity in the tumor-draining lymph node, with T and B cells, DCs, and macrophages coordinately increased (Fig. S5*C*).

Discussion

In multiple human tumor types, the clinical response to PD-1/PD-L1 blockade is highly variable among patients, with only a minority of patients achieving substantial, durable responses. In metastatic melanoma, clinical responses to anti–PD-1 antibodies correlate significantly with T cells in the tumor (1, 3, 18). This is consistent with retrospective studies in selected tumor types, demonstrating a strong association of T-cell content in tumors and overall survival (19). In addition, the degree of $CD3^+$ T-cell infiltration in melanoma correlates with the presence of type I IFN signature, which is associated with spontaneous remission of primary lesions (20) and increased survival in advanced melanoma (21).

The CT26 mouse tumor displays a similar heterogeneity in the response to PD-1 blockade, and the antitumor response correlates with IFN expression and T- and B-cell infiltration, suggesting utility of this model in evaluating therapies to increase responsiveness to anti–PD-1. A similar range of heterogeneity in these immune parameters was observed among tumors collected before anti–PD-1 treatment, suggesting that preexisting differences in the tumor microenvironment correlate with the response to PD-1 blockade as observed in human melanoma. The variability in anti–PD-1 response does not reflect systemic differences among mice, as only one of nine mice with two tumors rejected tumors on both flanks (Fig. 1*A*). Thus, the immunoregulatory state of each tumor may represent a stochastic event occurring early after tumor transplantation.

Responsiveness to PD-1 blockade is also associated with B cells and Ig gene expression. The five most highly up-regulated genes in responders compared with nonresponders were Ig genes and the B-cell chemoattractant CXCL13. Many clinical studies have shown a positive correlation between B cells and long-term survival in breast, colon, and nonsmall lung cancer (22–25). In other studies, the presence of B-cell signature correlates with responsiveness to IL-2 (26), ipilumimab (27), and anti-Her2/neu (28). We show that neutralization of CXCL13, which significantly decreased B-cell infiltration within the tumor (9) (Fig. S1*B*), diminished the response to anti–PD-1, suggesting that CXCL13 is a key chemokine contributing to anti–PD-1 effect. CXCL13 is a master chemokine able to organize ectopic lymphoid structures (25, 29, 30), and its neutralization may affect PD-1 blockade by destroying the organization of T-cell priming structures. A decrease in B-cell infiltration may also lead to a decrease in B-cell-mediated antigen presentation and costimulation for T cells (31–35).

Responsiveness to PD-1 blockade was completely lost when type I IFN signaling was blocked (Fig. 1). Type I IFNs have a

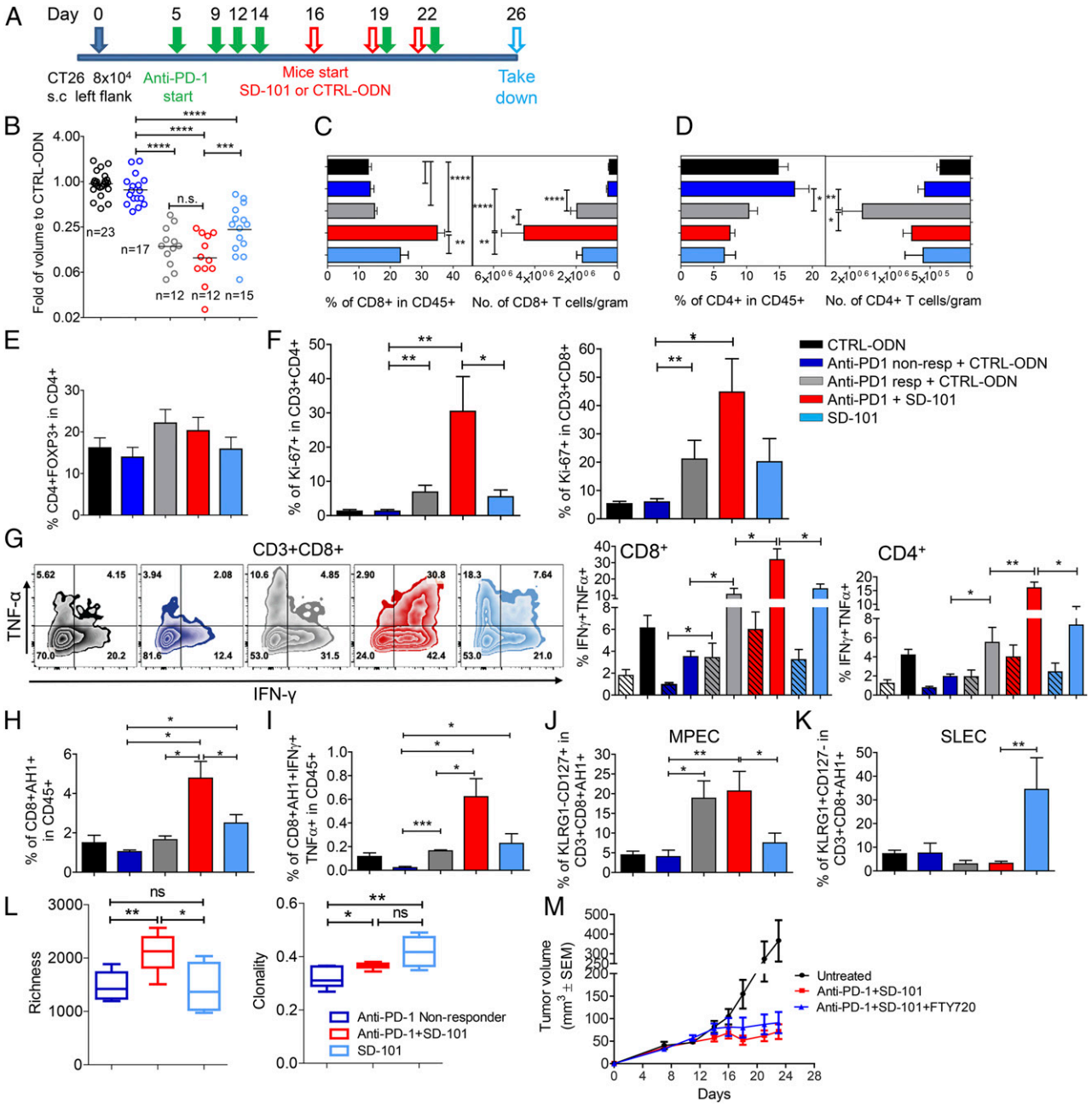

Fig. 5. SD-101 in combination with anti–PD-1 induces accumulation of polyfunctional T cell with increased clonality. (*A*) Treatment schedule scheme: Anti–PD-1 treatment started 5 d after tumor cell inoculation. After four anti–PD-1 injections, mice were randomized and received three intratumoral injections of SD-101 or CTRL-ODN on days 16, 19, and 22. A separate group of mice with the same tumor size, not pretreated with anti–PD-1, started receiving SD-101 alone. Tumors were harvested 4 d after last SD-101 or CTRL-ODN injection, on day 26. Anti–PD-1 responder status was defined as in Fig. 4. (*B*) Reduction in tumor volume relative to tumors treated with CTRL-ODN. For the anti–PD-1 responders group and anti–PD-1 plus SD-101 treated group, each point shown is an average of 5 to 10 tumors pooled together to obtain enough TILs to perform the assays; *n*, number of tumors or pools. Cumulative data are from six independent experiments. (*C* and *D*) Percentage of $CD8^+$ T cells among $CD45^+$ leukocytes and number of (*C*) $CD8^+$T cells or (*D*) $CD4^+$ T cells per gram of tumor tissue. (*E*) Percentage of Treg among CD4 T cells. TILs were extracted from samples shown in *B*. (*F*) Percentage of K_i-67^+ cells in $CD3^+CD4^+$ and $CD3^+CD8^+$ TILs cells. Cumulative data are from two independent experiments; *n* = three to five tumors or pool of tumors for anti–PD-1 responders and anti–PD-1 plus SD-101 treated groups. (G) TNF-α and IFN-γ production by $CD3^+CD4^+$ or $CD3^+CD8^+$ TILs after ex vivo stimulation. (*Left*) A representative contour plot. Tumor infiltrating leukocytes were stimulated for 3 h with PMA and Ionomycin in the presence of BFA (*Right*, open bars) or with BFA alone (*Right*, dashed bars). (*Right*) Cumulative data from five independent experiments, *n* = 19 to 21 tumors or pool of tumors for anti–PD-1 responders and anti–PD-1 plus SD-101 treated groups. (*H* and *I*) TNF-α and IFN-γ production by $CD8^+AH1^+$ TILs. TILs were incubated in vitro with BFA for 5 h, then stained and analyzed by FACS. (*H*) The percentage of $CD8^+AH1^+$ among $CD45^+$ TILs. (*I*) Percentage of $CD8^+AH1^+$ $IFN\gamma^+TNF\alpha^+$ among $CD45^+$ TILs. N. pools of tumors = 3–7 per group. Cumulative data are from 2 independent experiments. (*J* and *K*) Percentage of (*J*) MPEC and (*K*) SLEC in $CD8^+AH1^+$ gate. Number of tumors/pools of tumors = 4 to 11 per group. Cumulative data are from three independent experiments. (*L*) Productive unique TCRs and clonality by high-throughput quantitative sequencing of rearranged TCR-β genes of whole-tumor samples from mice treated with SD-101 alone (*n* = 4) or anti–PD-1 plus SD-101 (*n* = 6), and mice treated with anti–PD-1 but nonresponding (*n* = 6). (*M*) Antitumor activity of SD-101 plus anti–PD-1 does not require new T-cell migration. Tumor growth of CT26-bearing mice treated with anti–PD-1 plus SD-101 treatment in the absence or presence of FTY720 given 2 h before each SD-101 treatment is shown, with mean of 10 mice per group ± SEM. Schedule of treatment is as in Fig. S5. $*P \leq 0.05$; $**P \leq 0.01$; $***P \leq 0.001$; $****P \leq 0.0001$.

central role in shaping the antitumor response and influence multiple aspects of the immune system through recruitment and functional activation of T cells, B cells, and NK cells (8). In mouse models, ablation of type I IFN production decreased rejection of immunogenic tumor cells due to impaired ability of DC to cross-prime tumor-associated antigens to CTLs (cytotoxic T lymphocytes) (36, 37). In models of NK-mediated tumor rejection, production of type I IFN was essential to activate NK cytotoxicity (38). Here we demonstrate that early production of type I IFN is essential for the generation of tumor antigen-specific T cells, which are subsequently licensed by PD-1 blockade to reject tumors.

The ability of the CpG-C class ODN, SD-101, to induce high levels of type I IFN, T-cell-tropic chemokines, and DC maturation suggests that intratumoral administration of SD-101 could stimulate a set of changes in the tumor environment that would increase responsiveness to PD-1 blockade. Intratumoral SD-101 can substantially increase the frequency of complete rejection of three tumor lines in anti–PD-1 treated mice, both in the injected tumor and tumors at distant, uninjected sites. This demonstrates that, in the presence of anti–PD-1, SD-101 converts tumors into an effective vaccination, generating a systemic T-cell response able to infiltrate untreated tumor sites. Although mechanistic studies focused on the CT26 tumor, therapeutic efficacy of the combination was also observed with the TSA and MCA38 models, which show little response to PD-1 blockade alone.

The SD-101-induced antitumor response in anti–PD-1 nonresponders was dependent on $CD8^+$ but not $CD4^+$ T cells (Fig. 5 *F* and *G*). CD4-depleted mice that rejected (Fig. 2*F*) were still able to reject a subsequent challenge at day 80, suggesting generation of durable $CD8^+$ T-cell memory in the absence of $CD4^+$ T cells. This lack of dependence on $CD4^+$ T cells contrasts with previous reports that $CD4^+$ T cells are essential for $CD8^+$ T memory generation in cancer models (39, 40). The memory response can be restored by administering anti–PD-L1 blocking Ab in a setting in which $CD8^+$ T-cell priming is forced to happen in a helper-deficient host, suggesting that PD-1 blockade might have circumvented the requirement of help in our system (41).

The CT26 model is particularly suitable for studying factors in the tumor microenvironment that determine responsiveness to PD-1 blockade and the ability of a locally applied TLR9 agonist to change the microenvironment. Injection of SD-101 into anti–PD1-treated tumors significantly enhanced infiltration of $CD8^+$ T cells, relative to tumors from all groups, including tumors responding to the anti–PD-1 as monotherapy. The superior $CD8^+$ T-cell expansion likely reflects both recruitment and expansion at the tumor site. Gene expression profiling showed increased significance of GO terms, suggesting increased leukocyte adhesion and migration and chemokine production in the anti–PD-1 plus SD-101 group (Fig. 4*E* and Fig. S3*A*). Additionally, the SD-101 plus anti–PD-1 group had a significant increase in the proportion of $CD8^+$ $KI67^+$ cells, as well as GO terms, indicating activated T-cell proliferation (Fig. 4*F* and Fig. S3*A*). Proliferating $CD8^+$ T cells in the combination group were also more polyfunctional, with a higher fraction producing both IFN-γ and TNF-α (Fig. 5*G*), a characteristic associated with an increased ability to reject tumors (42–44). Thus, the combination was significantly more effective than either single agent at reversing the exhausted phenotype of tumor-specific $CD8^+$ T cells.

SD-101 alone directed tumor-specific $CD8^+$ T cells toward a $CD127^{low}KLRG1^{high}$ terminally differentiated phenotype, SLEC, previously shown to possess a limited life span (45) (Fig. 5*J*). This may help explain the lack of durability of SD-101 effects, despite substantial initial effects on tumor growth. In contrast, $CD8^+$ T cells in tumors responding to anti–PD-1 or the combination have the opposite phenotype, $CD127^{high}$ $KLRG1^{low}$, which defines cells able to survive and become memory cells (MPEC) (46) (Fig. 5*J*). High levels of t-box transcription factor (T-bet) induce SLEC differentiation, and CpGs can induce T-bet through IL-12 and IFN induction (45). PD-1 blockade has been shown to decrease T-bet in vaccine-induced $CD8^+$ T cells, promoting MPEC formation (47), and our findings demonstrate that PD-1 blockade can correct the CpG-mediated differentiation of effector T cells into short-lived cells.

In summary, our results support the use of intratumoral treatment with high interferogenic TLR9 agonists in patients unresponsive to anti–PD-1 to alter the tumor microenvironment, enhance priming of tumor antigen-specific T cells, and increase rate of response to treatment. Even in patients who respond to anti–PD-1 therapy, intratumoral SD-101 might generate and expand a more functional T-cell response, increasing the efficacy and durability of clinical response.

Materials and Methods

Mice. Female BALB/c mice or C57BL/6 (6 wk to 8 wk of age) were supplied by Harlan and housed at Murigenics. All experimental procedures involving live animals were approved by the Institutional Animal Care and Use Committees of Murigenics.

Statistical Analysis. All statistical analyses were performed using Prism software v5 (GraphPad Software). Differences were considered significant at a P level less than 0.05. Data were analyzed using unpaired Mann Whitney Student's t test, unless otherwise indicated in figure legends. P values were as follows: $^*P \le 0.05$, $^{**}P \le 0.01$, $^{***}P \le 0.001$, and $^{****}P \le 0.0001$.

Detailed materials and methods are provided in *SI Materials and Methods*.

ACKNOWLEDGMENTS. We thank the team at Murigenics for assistance with animal work and thank our colleagues at Dynavax for critical reading of the manuscript.

1. Smyth MJ, Ngiow SF, Ribas A, Teng MW (2016) Combination cancer immunotherapies tailored to the tumour microenvironment. *Nat Rev Clin Oncol* 13(3): 143–158.
2. Herbst RS, et al. (2014) Predictive correlates of response to the anti-PD-L1 antibody MPDL3280A in cancer patients. *Nature* 515(7528):563–567.
3. Tumeh PC, et al. (2014) PD-1 blockade induces responses by inhibiting adaptive immune resistance. *Nature* 515(7528):568–571.
4. Marabelle A, Kohrt H, Caux C, Levy R (2014) Intratumoral immunization: A new paradigm for cancer therapy. *Clin Cancer Res* 20(7):1747–1756.
5. Brody JD, et al. (2010) In situ vaccination with a TLR9 agonist induces systemic lymphoma regression: A phase I/II study. *J Clin Oncol* 28(28):4324–4332.
6. Kim YH, et al. (2012) In situ vaccination against mycosis fungoides by intratumoral injection of a TLR9 agonist combined with radiation: A phase 1/2 study. *Blood* 119(2):355–363.
7. Legler DF, et al. (1998) B cell-attracting chemokine 1, a human CXC chemokine expressed in lymphoid tissues, selectively attracts B lymphocytes via BLR1/CXCR5. *J Exp Med* 187(4):655–660.
8. Zitvogel L, Galluzzi L, Kepp O, Smyth MJ, Kroemer G (2015) Type I interferons in anticancer immunity. *Nat Rev Immunol* 15(7):405–414.
9. Ammirante M, Luo JL, Grivennikov S, Nedospasov S, Karin M (2010) B-cell-derived lymphotoxin promotes castration-resistant prostate cancer. *Nature* 464(7286):302–305.
10. Henry RA, Kendall PL (2010) CXCL13 blockade disrupts B lymphocyte organization in tertiary lymphoid structures without altering B cell receptor bias or preventing diabetes in nonobese diabetic mice. *J Immunol* 185(3):1460–1465.
11. Rusinova I, et al. (2013) Interferome v2.0: An updated database of annotated interferon-regulated genes. *Nucleic Acids Res* 41(Database issue):D1040–D1046.
12. Shinall SM, Gonzalez-Fernandez M, Noelle RJ, Waldschmidt TJ (2000) Identification of murine germinal center B cell subsets defined by the expression of surface isotypes and differentiation antigens. *J Immunol* 164(11):5729–5738.
13. Wherry EJ, Blattman JN, Murali-Krishna K, van der Most R, Ahmed R (2003) Viral persistence alters CD8 T-cell immunodominance and tissue distribution and results in distinct stages of functional impairment. *J Virol* 77(8):4911–4927.
14. Wei F, et al. (2013) Strength of PD-1 signaling differentially affects T-cell effector functions. *Proc Natl Acad Sci USA* 110(27):E2480–E2489.
15. Ahlers JD, Belyakov IM (2010) Memories that last forever: Strategies for optimizing vaccine T-cell memory. *Blood* 115(9):1678–1689.
16. Halin C, et al. (2005) The S1P-analog FTY720 differentially modulates T-cell homing via HEV: T-cell-expressed S1P1 amplifies integrin activation in peripheral lymph nodes but not in Peyer patches. *Blood* 106(4):1314–1322.
17. Spranger S, et al. (2014) Mechanism of tumor rejection with doublets of CTLA-4, PD-1/PD-L1, or IDO blockade involves restored IL-2 production and proliferation of $CD8^+$ T cells directly within the tumor microenvironment. *J Immunother Cancer* 2:3.

18. Teng MW, Ngiow SF, Ribas A, Smyth MJ (2015) Classifying cancers based on T-cell infiltration and PD-L1. *Cancer Res* 75(11):2139–2145.
19. Angell H, Galon J (2013) From the immune contexture to the Immunoscore: The role of prognostic and predictive immune markers in cancer. *Curr Opin Immunol* 25(2):261–267.
20. Vermi W, et al. (2011) Spontaneous regression of highly immunogenic *Molluscum contagiosum* virus (MCV)-induced skin lesions is associated with plasmacytoid dendritic cells and IFN-DC infiltration. *J Invest Dermatol* 131(2):426–434.
21. Bald T, et al. (2014) Immune cell-poor melanomas benefit from PD-1 blockade after targeted type I IFN activation. *Cancer Discov* 4(6):674–687.
22. Germain C, et al. (2014) Presence of B cells in tertiary lymphoid structures is associated with a protective immunity in patients with lung cancer. *Am J Respir Crit Care Med* 189(7):832–844.
23. Bedognetti D, Wang E, Marincola FM (2014) Meta-analysis and metagenes: CXCL-13-driven signature as a robust marker of intratumoral immune response and predictor of breast cancer chemotherapeutic outcome. *OncoImmunology* 3:e28727.
24. Bindea G, et al. (2013) Spatiotemporal dynamics of intratumoral immune cells reveal the immune landscape in human cancer. *Immunity* 39(4):782–795.
25. Germain C, Gnjatic S, Dieu-Nosjean MC (2015) Tertiary lymphoid structure-associated B cells are key players in anti-tumor immunity. *Front Immunol* 6:67.
26. Weiss GR, et al. (2011) Molecular insights on the peripheral and intratumoral effects of systemic high-dose rIL-2 (aldesleukin) administration for the treatment of metastatic melanoma. *Clin Cancer Res* 17(23):7440–7450.
27. Ji RR, et al. (2012) An immune-active tumor microenvironment favors clinical response to ipilimumab. *Cancer Immunol Immunother* 61(7):1019–1031.
28. Alistar A, et al. (2014) Dual roles for immune metagenes in breast cancer prognosis and therapy prediction. *Genome Med* 6(10):80.
29. Jones GW, Jones SA (2016) Ectopic lymphoid follicles: Inducible centres for generating antigen-specific immune responses within tissues. *Immunology* 147(2):141–151.
30. Dieu-Nosjean MC, Goc J, Giraldo NA, Sautès-Fridman C, Fridman WH (2014) Tertiary lymphoid structures in cancer and beyond. *Trends Immunol* 35(11):571–580.
31. Coughlin CM, Vance BA, Grupp SA, Vonderheide RH (2004) RNA-transfected CD40-activated B cells induce functional T-cell responses against viral and tumor antigen targets: implications for pediatric immunotherapy. *Blood* 103(6):2046–2054.
32. Yuseff MI, Pierobon P, Reversat A, Lennon-Duménil AM (2013) How B cells capture, process and present antigens: A crucial role for cell polarity. *Nat Rev Immunol* 13(7):475–486.
33. Ahmadi T, Flies A, Efebera Y, Sherr DH (2008) CD40 ligand-activated, antigen-specific B cells are comparable to mature dendritic cells in presenting protein antigens and major histocompatibility complex class I- and class II-binding peptides. *Immunology* 124(1):129–140.
34. DiLillo DJ, Yanaba K, Tedder TF (2010) B cells are required for optimal $CD4^+$ and $CD8^+$ T cell tumor immunity: Therapeutic B cell depletion enhances B16 melanoma growth in mice. *J Immunol* 184(7):4006–4016.
35. Homann D, et al. (1998) Evidence for an underlying CD4 helper and CD8 T-cell defect in B-cell-deficient mice: Failure to clear persistent virus infection after adoptive immunotherapy with virus-specific memory cells from muMT/muMT mice. *J Virol* 72(11):9208–9216.
36. Fuertes MB, et al. (2011) Host type I IFN signals are required for antitumor $CD8^+$ T cell responses through $CD8\alpha^+$ dendritic cells. *J Exp Med* 208(10):2005–2016.
37. Diamond MS, et al. (2011) Type I interferon is selectively required by dendritic cells for immune rejection of tumors. *J Exp Med* 208(10):1989–2003.
38. Swann JB, et al. (2007) Type I IFN contributes to NK cell homeostasis, activation, and antitumor function. *J Immunol* 178(12):7540–7549.
39. Gao FG, et al. (2002) Antigen-specific $CD4^+$ T-cell help is required to activate a memory $CD8^+$ T cell to a fully functional tumor killer cell. *Cancer Res* 62(22):6438–6441.
40. Antony PA, et al. (2005) $CD8^+$ T cell immunity against a tumor/self-antigen is augmented by $CD4^+$ T helper cells and hindered by naturally occurring T regulatory cells. *J Immunol* 174(5):2591–2601.
41. Kim J, et al. (2015) Memory programming in $CD8^+$ T-cell differentiation is intrinsic and is not determined by CD4 help. *Nat Commun* 6:7994.
42. Imai N, Ikeda H, Tawara I, Shiku H (2009) Tumor progression inhibits the induction of multifunctionality in adoptively transferred tumor-specific $CD8^+$ T cells. *Eur J Immunol* 39(1):241–253.
43. Aranda F, et al. (2011) Adjuvant combination and antigen targeting as a strategy to induce polyfunctional and high-avidity T-cell responses against poorly immunogenic tumors. *Cancer Res* 71(9):3214–3224.
44. Yuan J, et al. (2008) CTLA-4 blockade enhances polyfunctional NY-ESO-1 specific T cell responses in metastatic melanoma patients with clinical benefit. *Proc Natl Acad Sci USA* 105(51):20410–20415.
45. Joshi NS, et al. (2007) Inflammation directs memory precursor and short-lived effector $CD8^+$ T cell fates via the graded expression of T-bet transcription factor. *Immunity* 27(2):281–295.
46. Kaech SM, et al. (2003) Selective expression of the interleukin 7 receptor identifies effector CD8 T cells that give rise to long-lived memory cells. *Nat Immunol* 4(12):1191–1198.
47. Duraiswamy J, Kaluza KM, Freeman GJ, Coukos G (2013) Dual blockade of PD-1 and CTLA-4 combined with tumor vaccine effectively restores T-cell rejection function in tumors. *Cancer Res* 73(12):3591–3603.
48. Marshall JD, et al. (2005) Superior activity of the type C class of ISS in vitro and in vivo across multiple species. *DNA Cell Biol* 24(2):63–72.
49. Guiducci C, et al. (2013) RNA recognition by human TLR8 can lead to autoimmune inflammation. *J Exp Med* 210(13):2903–2919.
50. Guiducci C, et al. (2010) Autoimmune skin inflammation is dependent on plasmacytoid dendritic cell activation by nucleic acids via TLR7 and TLR9. *J Exp Med* 207(13):2931–2942.